Journal of Materials Chemistry C

Accepted Manuscript

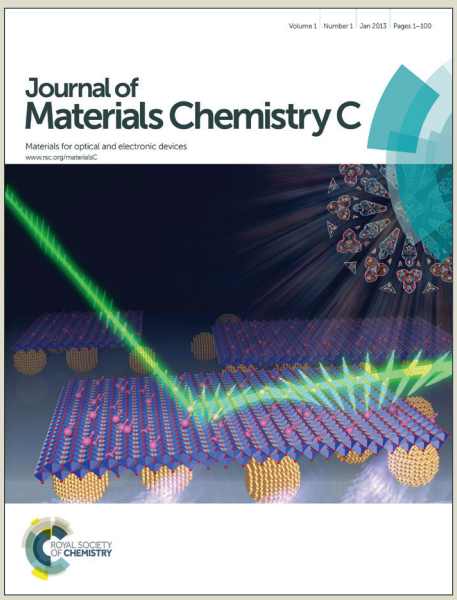

ROYAL SOCIETY OF CHEMISTRY

www.rsc.org/materialsC

Journal Name

RSCPublishing

ARTICLE

Lanthanide ions (Eu^{3+}, Tb^{3+}, Sm^{3+}, Dy^{3+}) activated ZnO embedded zinc 2,5-pridinedicarboxylic metal organic frameworks for luminescent application

Cite this: DOI: 10.1039/x0xx00000x

Received 00th January 2012,
Accepted 00th January 2012

DOI: 10.1039/x0xx00000x

www.rsc.org/

Tian-Wei Duan and Bing Yan*

A series of hybrids based on lanthanide ions activated zinc metallic organic framework of 2,5-pyridinedicarboxylate (ZnO@Zn(pdc)-Ln, Ln = Eu, Tb, Sm, Dy) have been synthesized by coordination reaction under solvothermal conditions. Zinc oxide is formed in the framework of lanthanide doped zinc centered MOFs due to decomposition of zinc compounds caused by alkaline environment and high-temperature. Furthermore, mechanism of zinc oxide formation is discussed in our work. Structure, composition and morphology of obtained materials are characterized by XRD, FTIR, ICP and SEM. Photophysical properties of these hybrid materials are investigated in details and reveal that characteristic emission line of corresponding Ln^{3+} ion is appeared under ultraviolet radiation. Besides, Eu^{3+} ions activated ZnO@Zn(pdc) features white light under the ultraviolet excitation, which shows the possibility to be exploited as WLED.

1. Introduction

Metal−organic frameworks (MOFs) exhibit versatile properties derived from their uniform and porous structure.[1] In addition to the most interested area of gas storage,[2] luminescence application of MOFs has developed rapidly in recent years.[3] Luminescent MOFs can be designed to have different emissive properties, which are highly desirable for sensing,[4] biomedical analysis[5] and lighting devices.[6] There are several ways to achieve fluorescence in MOFs,[7] that is generated from intra-ligand charge transfer, metal to ligand charge transfer (MLCT), ligand to metal charge transfer (LMCT), 4f→4f transition of lanthanide or guest molecule emission. Favourable luminescence properties of MOFs or their hybrid materials render them attractive in the field of white light emission.[8] White-light-emitting materials and devices have attracted much attention because of their potential applications in, for instance, solid-state lighting (SSL), full-color displays, and backlights. Lanthanide activated MOFs are extensively studied for decades, since their virtues of high colour purity, high luminescence quantum efficiencies and a wide range of lifetimes. Besides, several advantages of MOFs make them useful for sensitizing lanthanide cations.[9] One reason is that well defined structures of MOFs incorporate a large number of chromophoric sensitizers and lanthanide ions, which result in a large number of photons emitted per unit volume. Another is that MOF structures can be tailored to modulate and optimize the photoluminescence properties of lanthanide cations.

Generally, MOFs with single lanthanide luminescence centre only emit characteristic lanthanide emission line. Sometimes, inclusion of more than one luminescent centre in MOF materials leads to various luminescence performances.[10] In addition, compared with pure MOFs, the heterostructures integrating MOFs with other functional materials show great advantages due to their synergism effect. In early studies, semiconductor nanoparticles (e.g. CdS and ZnO) are conventional compounds to embed in the cavities of porous silicate and shows remarkable luminescence properties.[11] Predictably, such semiconductor@MOFs heterostructures should have potential application in photoluminescence (PL) devices.[12] Particularly, nanoparticles have been incorporated into microporous structure through chemical vapour deposition,[13] liquid/incipient wetness impregnation[14] and microwave irradiation.[15] For many decades, ZnO as a kind of semiconductor has always been the research focus, not only for its remarkable photoelectric properties but also for photoluminescent properties[16]. To the best of our knowledge, formation of ZnO is not a singular thing in zinc metal organic framework. In earlier times, Bordiga and coworkers[17] found that luminescence properties of one zinc metal organic framework, namely MOF-5, presented much more like ZnO QDs'. They believed that the organic part act as a photon

antenna able to efficiently transfer the energy to the inorganic ZnO-like QDs part (Zn_4O_{13} cluster). However, after that Allendorf and co-workers[18] cast doubt on previous reports of MOF-5 as a semiconductor, as all previous observations may be explained by the presence of ZnO impurities serving as the photocatalytic and semiconducting species. They found various synthesis method results in different impurity of MOF-5 by the means of photoluminescence spectroscopy, and it is hard to avoid formation of ZnO via direct-mixing precipitation method and solvothermal crystallization syntheses. The fact is that ZnO phase is readily available in the system with zinc source and alkaline environment. Since then, some scientists became interest in fabricate ZnO from zinc metal organic framework source. Up till now, it is possible to realize ZnO nanorods embedded on a ZIF-8 matrix[19] and achieve metal-doped rectangular ZnO nanocrystals from metal insert nano MOF-5.[20] In this article, we present that zinc oxide embedded metal organic framework (ZnO@Zn(pdc)) can be obtained via solvothermal method under the temperature of 180 ^oC. The structure of MOF in this experiment is zinc atoms linked to nitrogen atoms and oxygen atoms of 2,5-pridinedicarboxylic acid forming a microporous construction. Since mechanism of ZnO forming is in relation to the alkaline environment created by deformation of DMF, once heating temperature reaches deformation temperature of DMF, ZnO phase start to come into being. Moreover, we can acquire various emission light via incorporating lanthanide into ZnO loaded MOF. Lanthanide ions (Eu^{3+}, Tb^{3+}, Sm^{3+}, Dy^{3+}) activated ZnO shows distinct characterize emission under ultraviolet excitation. In addition to that, Eu activated MOF displays interesting white-light emission under near ultraviolet excitation. The resulting Eu activated MOF can acquire white-light emission through a dual-emitting pathway: the metal-centered (MC) f−f emission characteristic of Ln^{3+} ion and defect emission of ZnO. Furthermore, obtained white light emission materials (ZnO@Zn(pdc)-Eu) which show the CIE coordinates of (0.35, 0.41) and the quantum efficiency of 10.2 % under the excitation of 375 nm, can be fabricated into WLED for potential utility.

2. Experiment

2.1 Materials

$Eu(NO_3)_3·6H_2O$, $Tb(NO_3)_3·6H_2O$, $Sm(NO_3)_3·6H_2O$, $Dy(NO_3)_3·6H_2O$ were obtained from corresponding oxides in HNO_3, and the other chemicals purchased were analytically pure and used without further purification.

2.2 Synthesis of $[Zn_2(pdc)_2(dmf)_2]_n·ndmf$

Synthesis of $[Zn_2(pdc)_2(dmf)_2]_n·ndmf$ is followed the procedure in literature.[21] 0.0509 g (0.305 mmol) 2,5-pridinedicarboxylic acid (H_2pdc) was dissolved in 5 mL N,N-dimethylformamide (DMF) under ambient conditions. Then $Zn(NO_3)_2·6H_2O$ (0.2359 g, 0.793 mmol) DMF solution (5 mL) was added to the clear solution of the organic acid dropwise. The mixture was further stirred for 30 min in a 50-mL solvothermal vessel and was heated to 80 °C for 12 hrs. The resulting white solid was centrifuged, and washed with DMF for three times. The product was then dried under a vacuum for 12 hrs. As-synthesized samples are denoted as Zn(pdc)-1.

2.3 Study of ZnO formation in $[Zn_2(pdc)_2(dmf)_2]_n·ndmf$

Study of ZnO formation in $[Zn_2(pdc)_2(dmf)_2]_n·ndmf$ is of a similar procedure as prepare $[Zn_2(pdc)_2(dmf)_2]_n·ndmf$. Obtained precursor was further stirred for 30 min in a 50-mL solvothermal vessel and was heated to 100, 120, 140, 160 and 180 °C for 12 hrs, respectively. The resulting white solid was centrifuged, and washed with DMF for three times. The product was then dried under a vacuum for 12 hrs. As-synthesized samples are denoted as Zn(pdc)-2, Zn(pdc)-3, Zn(pdc)-4, Zn(pdc)-5, Zn(pdc)-6.

2.4 Synthesis of lanthanide functionalized $[Zn_2(pdc)_2(dmf)_2]_n·ndmf$

A similar process was employed to prepare lanthanide functionalized $[Zn_2(pdc)_2(dmf)_2]_n·ndmf$, except for adding a certain amount of 5 mol% $Ln(NO_3)_3·6H_2O$ (Ln = Eu, Tb, Sm, Dy) into the precursor solution at the initial stage, while other reaction parameters were kept unchanged. The product was collected by centrifugation, washed several times with dmf, and dried under vacuum for characterization. We denote the synthesized lanthanide functionalized $[Zn_2(pdc)_2(dmf)_2]_n·ndmf$ as ZnO@Zn(pdc)-Eu, ZnO@Zn(pdc)-Tb, ZnO@Zn(pdc)-Sm, ZnO@Zn(pdc)-Dy.

2.5 Fabrication of white light emission diode

By a simple and efficient dip coating procedure, a thin film of ZnO@Zn(pdc)-Eu can be applied onto a commercially available UV-LED lamp, and thus accomplish the conversion into a new LED that emits bright white light. Specifically, an as-made crystalline sample of ZnO@Zn(pdc)-Eu (about 10 mg) was loaded into an agate mortar and manually ground with the pestle for 10 min to afford a fine powder. Ethanol (0.5 mL) was then added to the mortar. Further grinding (for about 2 min) was applied until a homogeneous slurry was achieved. A commercial 375 nm UV-LED lamp was then dipped into the slurry, held therein for several seconds, and then taken out for the coating to dry in air.

2.6 Characterization

Infrared spectra were measured within KBr pellets from 4000 to 400 cm^{-1} using a Nexus 912 AO446 Fourier transform infrared spectrum radiometer (FTIR). X-ray powder diffraction patterns (XRD) were acquired on Rigaku D/max-rB diffractometer equipped with Cu anode; the data were collected within the 2θ range of 5-75°. TGA were performed on a Netzsch STA 449C system with the heating rate of 5 °C/min in nitrogen atmosphere. The morphology of the samples was inspected using a scanning electron microscope (SEM, Philips XL-30). The ultraviolet diffusion reflection spectra of the powdered samples were recorded by a B&WTEK BWS003 spectrophotometer. Luminescence excitation spectra and emission spectra were measured on an Edinburgh FLS920 fluorescence spectrometer. The lifetime measurements were measured on an Edinburgh Instruments FLS 920 fluorescence spectrometer using microsecond (100 mW) lamp. The outer luminescent quantum efficiency was determined using an integrating sphere (150 mm diameter, $BaSO_4$ coating) from Edinburgh FLS920 phosphorimeter. The spectra were corrected for variations in the output of the excitation source and for variations in the detector response. The quantum yield can be defined as the integrated intensity of the luminescence signal divided by the integrated intensity of the

absorption signal. The absorption intensity was calculated by subtracting the integrated intensity of the light source with the sample in the integrating sphere from the integrated intensity of the light source with a blank sample in the integrating sphere. All of the measurements were performed at room temperature.

3. Results and discussion

3.1 Study of formation of ZnO inside metal organic framework

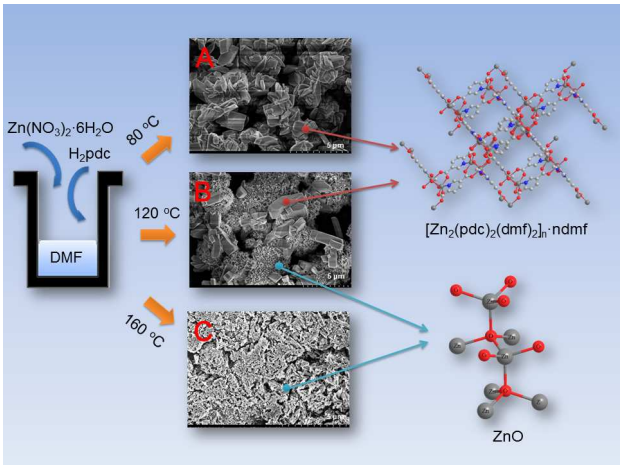

Scheme 1 Illustration of temperature dependence of product morphology and composition; (A) Zn(pdc)-1, (B) Zn(pdc)-3, (C) Zn(pdc)-5.

The investigation of ZnO formation inside MOF is showed in Scheme 1. Zn(pdc)-1 was synthesized through a solvothermal method. The XRD pattern of as-synthesized product is in accordance with that of $[Zn_2(pdc)_2(dmf)_2]_n$·ndmf (Figure S1), which indicates that the crystalline structure of Zn(pdc)-1 is monoclinic with $P2_1/n$ space group. The coordination zinc ions of $[Zn_2(pdc)_2(dmf)_2]_n$·ndmf can be classified into two types: one is five-coordinated by one N and four O atoms from three pdc ligands; another one is six-coordinated by one N and five O atoms from four pdc and one DMF ligands. Actually, voids in $[Zn_2(pdc)_2(dmf)_2]_n$·ndmf form continuous two-dimensional nets parallel to the (101) plane.

When reaction temperature increases, however, structural destruction of Zn(pdc)-1 comes about along with formation of ZnO in the system. The X-ray powder diffraction (XRD) pattern of temperature dependent products in Figure 1 shows that the structure of MOF keeps intact under the temperature of 120 °C and gradually collapse with the rising temperature. Newly appeared diffraction peaks can be well indexed to the hexagonal wurtzite ZnO (JCPDS card, No. 99-0111). Hence, phase changes in reaction system cause changes in morphology of product in the system. SEM pictures in Scheme 1 (A, B, C) illustrate the morphologies of the as-synthesized products at the temperature of 80 °C, 120 °C and 160 °C, respectively. It is shown that the structure of Zn(pdc)-1 is in blocks of irregular shape under the temperature of 80 °C (Scheme 1A). With the temperature up to 120 °C, Zn(pdc)-3 exhibits grass-like morphology distributed on the bulk structure of MOF, which could be due to formation of less ZnO (Scheme 1B). As the system heats at 160 °C, the morphology of Zn(pdc)-6 presents rod-like morphology with manifest agglomeration owning to a large amount of ZnO forming (Scheme 1C). Fourier transform infrared (FTIR) spectroscopy (Figure S2) exhibited peaks at 1660 cm^{-1} [ν_{asym} (CO_2^-)], 1616 cm^{-1} [ν_{asym} (CO_2^-)], 1396 cm^{-1} [ν_{sym} (CO_2^-)], and 1359 cm^{-1} [ν_{asym} (CO_2^-)]. Besides, considering ZnO is a Raman active substance, we adopt Raman spectra to confirm the existence of ZnO. Raman spectra of Zn(pdc)-2 (synthesized at 100 °C) and Zn(pdc)-6 (synthesized at 180 °C) are shown in Figure S3. In the spectrum of Zn(pdc)-2, it clearly shows that several peaks appear in the range 250~1750 cm^{-1} due to the vibration of $[Zn_2(pdc)_2(dmf)_2]_n$·ndmf frameworks. However, with synthesis temperature rising, it obviously shows three asymmetric LO multiphonon peaks of ZnO at 595 and 1082 and 1665 cm^{-1} in the Raman spectrum of Zn(pdc)-6. Thus, it confirms that ZnO phase is formed at 180 °C.

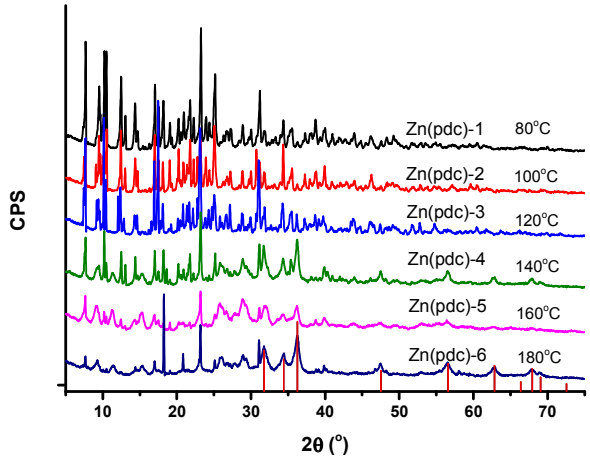

Figure 1 XRD patterns of Zn(pdc)-1, Zn(pdc)-2, Zn(pdc)-3, Zn(pdc)-4, Zn(pdc)-5, Zn(pdc)-6. The insert red bars are the standard diffraction lines of ZnO (JCPDS card, No. 99-0111).

In our experiment, the formation of ZnO is mainly due to the alkaline environment created by the decomposition of DMF under relatively high temperature (Eq. (1)).[22] Dimethylamine, one of the decomposition products, can be considered as an effective ligand for Zn^{2+} (Eq. (2)) and the hydrolytic equilibrium of the related complex controls overall ZnO growth, by a gradual release of Zn^{2+} and OH^- reactants. At the temperature of 120 °C, the $[Zn(CH_3)_2NH]^{2+}$ complex equilibrium is perturbed and dimethylamine undergoes basic hydrolysis (Eq. (3)) similar as the procedure of buffer effect.[23] Thus, when their ionic product (IP) exceeds the $Zn(OH)_2$ solubility product constant (K_{ps}) the precipitation of ZnO nuclei becomes activated, due to the presence of free Zn^{2+} and OH^- ions (Eq. (4)). Another fact that may prove the mechanism of dimethylamine controlled reaction is that there is a formation of ZnO superstructure (Figure S4A) only in the precursor of $Zn(NO)_3$ and DMF solution under 180°C. Figure S3B displays the nest like structure comprised of ZnO nanorods with the average width of 200 nm and length of 700 nm. This mesostructure material has a diameter of 10 μm. Furthermore, the XRD pattern of resulted product confirms that the material is consisted of ZnO with nanostructure (Figure S5).

$$HCON(CH_3)_2 + H_2O \rightarrow (CH_3)_2NH + HCOOH \quad (1)$$

$$Zn^{2+} + (CH_3)_2NH \rightleftharpoons [Zn(CH_3)_2NH]^{2+} \quad (2)$$

$$(CH_3)_2NH + H_2O \rightleftharpoons (CH_3)_2NH_2^+ + OH^- \quad (3)$$

$$Zn^{2+} + 2OH^+ \rightarrow Zn(OH)_2 \downarrow \rightarrow ZnO \downarrow + H_2O \quad (4)$$

According to Figure S6, excitation spectrum of H_2pdc ligand presents a broad peak centered at 425 nm, which can be attributed to electron transition from single state to triple state. When excited at 400 nm, H_2pdc displays a broad emission peak centered at 515 nm. However, introduction of zinc ions in H_2pdc forming a structure of frameworks causes the marvelous changes in the excitation and emission spectra, which show apparently blue shift compared to the ligand spectra. Due to the coordination of zinc atom to the oxygen and nitrogen atoms of H_2pdc, ligand to metal charge transfer (LMCT) becomes a dominated factor in the emission of $[Zn_2(pdc)_2(dmf)_2]_n \cdot ndmf$. The photoluminescence of temperature dependent products is influenced by the composition of products. Figure 2 presents the PL spectra of synthesized product under the temperature varied from 80 °C to 180 °C. It is obvious that the spectra of photoluminescence are in line with XRD patterns. Thus, below the temperature of 120 °C (Figure 2A) the dominant luminescence is mainly generated by LMCT from pdc ligand to zinc ion, while above 140 °C (Figure 2B) the dominant luminescence is almost entirely generated by defect emission of ZnO. One possible reason for the variations in the position of the excitation band and emission band among Zn(pdc)-1, Zn(pdc)-2 and Zn(pdc)-3 are reduction of LMCT resulted from gradually loss of zinc metal organic frameworks to form ZnO. Zn(pdc)-4, Zn(pdc)-5 and Zn(pdc)-6 share the similar spectra, which displays that the center of excitation band locate at 395 nm and emission band at 475 nm. These three analogous emission spectra are mainly due to the defect emissions of ZnO.[15] Furthermore, the excitation spectra are in accordance with Uv-vis DRS (Figure S7). In the UV-vis DRS, it clearly shows that absorbance at 370 nm of ZnO semiconductor absorption is enhanced with the rising temperature, indicating more ZnO formed in the system. The emission band centered at blue color region with excitation wavelength around near ultraviolet region is extremely beneficial to fabricate europium doped white light emission materials.[24]

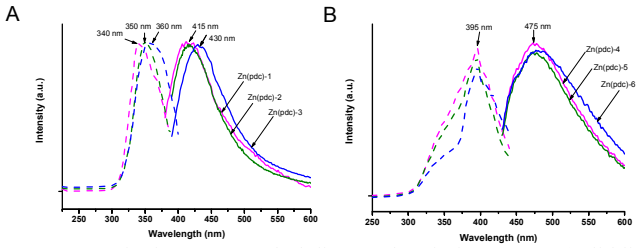

Figure 2 Excitation spectra (dash line) and emission spectra (solid line) of (A) Zn(pdc)-1, Zn(pdc)-2, Zn(pdc)-3; (B) Zn(pdc)-4, Zn(pdc)-5, Zn(pdc)-6.

3.2 Fabrication of lanthanide activated ZnO@Zn(pdc)

Lanthanide activated ZnO@Zn(pdc) was manufactured via solvothermal method under the temperature of 180 °C. The XRD pattern of lanthanide loaded ZnO@Zn(pdc) exhibits several peaks in 2θ ranged 5-55 ° (Figure 3), which matches pretty well with XRD pattern of simulated $[Zn_2(pdc)_2(dmf)_2]_n \cdot ndmf$.[20] Hence, it suggests that the ordered porous structure of zinc metal organic framework is conserved after the introduction of lanthanide ions (Figure 3) compared to zinc metal organic framework under relatively high temperature (Figure 1, Zn(pdc)-6). Furthermore, the presence of ZnO phase is also confirmed by XRD. The consistent XRD results indicate that introduction of doping lanthanide ions do not change the crystalline form. However, when lanthanide source is added into the precursor of zinc nitrate and pdc ligand, compared to ZnO@Zn(pdc) series, it is worth noting that there is no product under the temperature of 80-120 °C. This consequence can be attributed to coordination competition between lanthanide ions and zinc ions, which makes harder for zinc to fabricate frameworks. Relative high temperature, however, results in ZnO forming reaction in system, which can concert with construction reaction of frameworks and be able to overwhelm coordination energy barrier. The element analysis of ZnO@Zn(pdc)-Ln (Ln = Eu, Tb, Sm, Dy) are determined by ICP (Table S1). The results show that the doping ratio of Ln (Ln = Eu, Tb, Sm, Dy) to Zn are almost in accordance with the experiment doping mole ratio (Ln: Zn= 0.05). We can also deduce that lanthanide ions are successfully introduced into the frameworks.

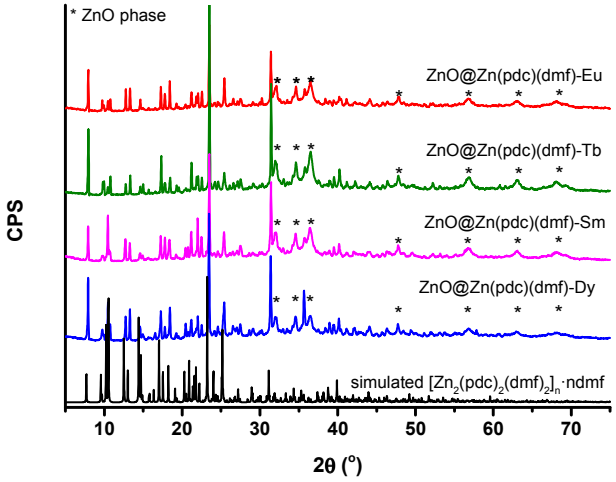

Figure 3 XRD patterns of ZnO@Zn(pdc)-Eu, ZnO@Zn(pdc)-Tb, ZnO@Zn(pdc)-Sm, ZnO@Zn(pdc)-Dy. The insert star marks (*) are assigned to diffraction peaks of ZnO phase.

The morphology of ZnO@Zn(pdc)-Ln (Ln = Eu, Tb, Sm, Dy) crystals was studied by scanning electron micrograph (Figure 4). As shown in Figure 4A and Figure 4B, the samples of ZnO@Zn(pdc)-Eu and ZnO@Zn(pdc)-Tb consist of cauliflower-like structure and bulk crystal, which can be referred as ZnO phase and lanthanide loaded zinc metal organic framework. Whereas the morphology of ZnO@Zn(pdc)-Sm and ZnO@Zn(pdc)-Dy (Figure 4C, 4D) shares the uniformed needle like structure. XRD peaks of resulting ZnO are wide, indicating the actual nanostructure of ZnO. Moreover, approximate size of nanostructure can be determined by Scherrer Equation (Eq. 5).

$$\tau = \frac{K\lambda}{FW(S)cos(\theta)} \quad (5)$$

Here τ is the mean size of the ordered crystalline domains, K is a dimensionless shape factor with a value close to unity, λ is the wavelength of X-ray, FW(S) is the line broadening at half the maximum intensity, and θ is the Bragg angle. According the Scherre equation (Eq. 5), the calculated size of five domain peaks shows that the nanocrystals characterize the nano dimension size as 10-20 nm (Table S2).

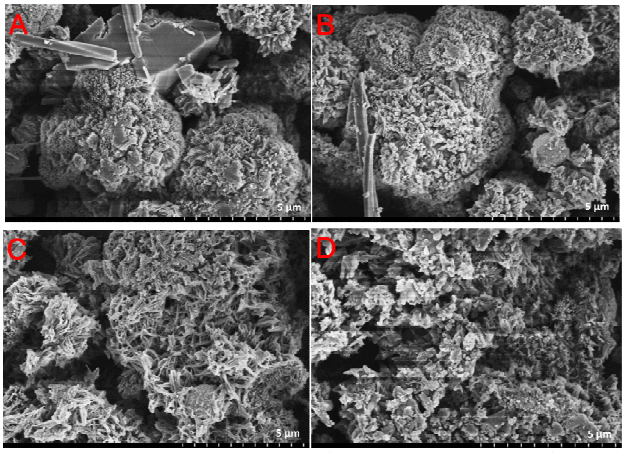

Figure 4 SEM pictures of (A) ZnO@Zn(pdc)-Eu, (B) ZnO@Zn(pdc)-Tb, (C) ZnO@Zn(pdc)-Sm, (D) ZnO@Zn(pdc)-Dy.

The emission spectrum of $[Zn_2(pdc)_2(dmf)_2]_n \cdot ndmf$ exhibits a broad peak centered at 430 nm when it is excited by the wavelength of 354 nm (Figure S5). Whereas, the emission spectra of ligand showed a broad peaks centered at 515 nm. The blue shift of emission peak is probably because zinc atoms disturb the luminescence of 2,5-pyridinedicarboxylic acid. The fluorescence excitation and emission spectra of the ZnO@Zn(pdc)-Ln (Ln = Eu, Tb, Sm, Dy) is displayed in Figure 5. It is clearly showed from the figures that all the excitation spectra (the dashed line) dominated by a broad absorption bands located at ultraviolet region centered at about 285 nm, suggesting that the resulted materials can absorb the ultraviolet light efficiently and then sensitize the emission of lanthanide by energy transfer. The luminescence of ZnO@Zn(pdc)-Ln is mainly attribute to the organic ligand's excited energy levels with a subsequent transfer to the resonant excited levels of lanthanide ions, and therefore yielding a final strong light emission. Furthermore, the emission spectra (the solid line) of ZnO@Zn(pdc)-Ln are obtained by using appropriate wavelength as excitation source, which display their characteristic emission peaks. The emission lines of ZnO@Zn(pdc)-Eu are assigned to $^5D_0 \rightarrow 7F_0$, $^5D_0 \rightarrow 7F_1$, $^5D_0 \rightarrow ^7F_2$, $^5D_0 \rightarrow ^7F_3$ and $^5D_0 \rightarrow ^7F_4$ transitions for those peaks located at about 579, 591, 616, 650, and 700 nm, respectively. It can be observed that the emission spectra shown in Figure 5A are dominated by a very intense $^5D_0 \rightarrow ^7F_2$ transition at 616 nm. It is well known that the $^5D_0 \rightarrow ^7F_2$ transition is a typical electric dipole transition and is very sensitive to the local symmetry of europium ions, while the parity-allowed magnetic dipole transition $^5D_0 \rightarrow ^7F_1$ is practically independent of the ions' surroundings. Hence, the intensity ratios $I(^5D_0 \rightarrow ^7F_2)/I(^5D_0 \rightarrow ^7F_1)$ (I_{02}/I_{01}) can be seen as an indicator for the local environment of ions. According to the calculated intensity ratio for 4.7, we concluded that the chemical environment around the europium ions is in low symmetry. For ZnO@Zn(pdc)-Tb, the emission lines depicted on the right of Figure 5B are assigned to $^5D_4 \rightarrow ^7F_6$, $^5D_4 \rightarrow ^7F_5$, $^5D_4 \rightarrow ^7F_4$ and $^5D_4 \rightarrow ^7F_3$ transitions for those peaks located at 489, 544, 583 and 621 nm, respectively. The emission peaks of ZnO@Zn(pdc)-Sm are assigned to $^4G_{5/2} \rightarrow ^6H_{5/2}$, $^4G_{5/2} \rightarrow ^6H_{7/2}$ and $^4G_{5/2} \rightarrow ^6H_{9/2}$ transitions for those peaks located at 562, 597, and 643 nm, respectively (Figure 5C). For ZnO@Zn(pdc)-Dy, the emission lines depicted on the right of Figure 5D are assigned to $^4F_{9/2} \rightarrow ^6F_{15/2}$ and $^4F_{9/2} \rightarrow ^6F_{13/2}$ transitions for those peaks located at 481 and 574 nm, respectively.

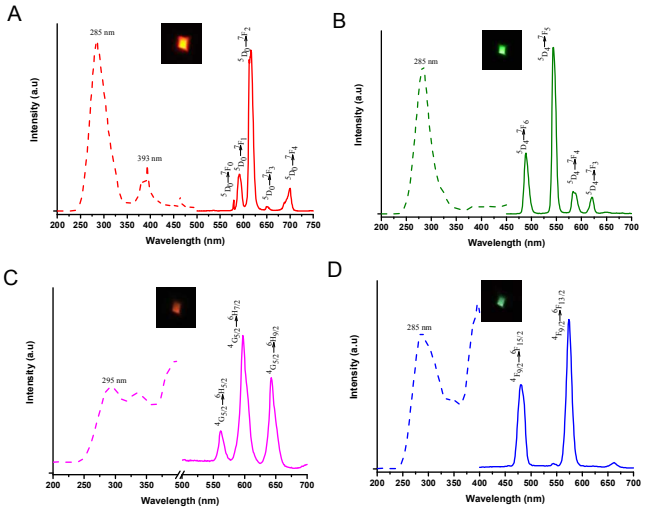

Figure 5 Excitation spectra (dash line) and emission spectra (solid line) of (A) ZnO@Zn(pdc)-Eu, (B) ZnO@Zn(pdc)-Tb, (C) ZnO@Zn(pdc)-Sm, (D) ZnO@Zn(pdc)-Dy.

For further investigation of the photoluminescence properties, we measured the luminescence lifetime decay of ZnO@Zn(pdc)-Ln at room temperature under the maximum excitation wavelength with the monitor wavelength of most intense emission, and the resulting lifetimes are given in Table 1. Europium and terbium activated ZnO@Zn(pdc) materials possess relatively high decay time. Besides, we measure efficiencies on an Edinburgh Instruments FLS 920 fluorescence spectrometer and the resulting emission quantum efficiencies are listed in Table 1.

Table 1 The luminescent efficiencies and lifetimes for ZnO@Zn(pdc)-Eu, ZnO@Zn(pdc)-Tb, ZnO@Zn(pdc)-Sm, ZnO@Zn(pdc)-Dy.

Materials	τ (μs)[a]	η (%)[b]
ZnO@Zn(pdc)(dmf)-Eu	377	35
ZnO@Zn(pdc)(dmf)-Tb	951	42
ZnO@Zn(pdc)(dmf)-Sm	18	9
ZnO@Zn(pdc)(dmf)-Dy	24	11

[a] lifetimes (τ) of $^5D_0$ energy level for Eu^{3+} excited state, $^5D_4$ energy level for Tb^{3+} excited state, $^4G_{5/2}$ energy level for Sm^{3+} excited state, $^4H_{9/2}$ energy level for Dy^{3+} excited state, respectively; [b] the luminescent quantum efficiencies are measured on an Edinburgh Instruments FLS 920 fluorescence spectrometer.

As displayed in Table 1, the quantum yields of ZnO@Zn(pdc)-Eu and ZnO@Zn(pdc)-Tb are reasonably high. As illustrated in The colors of the emissions can be better quantified with the CIE (Commission Internationale de l'Eclairage) chromaticity diagram, which serves to specify how the human eye perceives light with a given spectrum. Figure 6 shows that the CIE chromaticity coordinates for ZnO@Zn(pdc)-Ln fall in reddish orange, yellowish green, orange, and yellow green, respectively.Under 285 nm excitation, the luminescence of ZnO@Zn(pdc)-Eu and ZnO@Zn(pdc)-Tb are fairly bright. However, the luminescence of ZnO@Zn(pdc)-Sm and ZnO@Zn(pdc)-Dy are comparatively weak (Figure 5). It might be due to unmatchable energy level between the triple excitation state of 2,5-pyridinedicarboxylic acid and the excitation energy level of Sm^{3+} or Dy^{3+}.

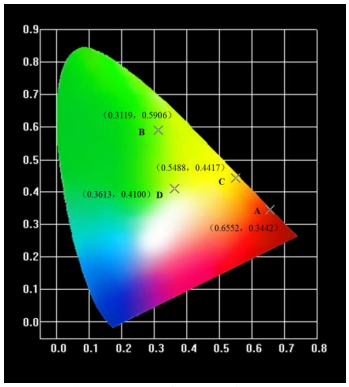

Figure 6 CIE diagram of (A) ZnO@Zn(pdc)-Eu, (B) ZnO@Zn(pdc)-Tb, (C) ZnO@Zn(pdc)-Sm, (D) ZnO@Zn(pdc)-Dy.

As also shown in Figure 7, the emissions of ZnO@Zn(pdc)-Eu respond similarity to the variation of traditional near-UV excitation wavelengths (365 nm, 375 nm, 395 nm). Under excitation at these near-UV excitations, the characteristic emission of the Eu^{3+} ion can be achieved (Figure 7A). Besides, a broad emission band from 420 nm to 550 nm can be ascribed to the emission of zinc matrix. For the consideration of used ZnO@Zn(pdc)-Eu as white light emission material, it would be necessary to determine the quantum efficiency under different excitations. The efficiency of powder sample of ZnO@Zn(pdc)-Eu can be achieved by quantum efficiency determined equation. It is well established that the emission quantum efficiency (η) of $^5D_0$ excited state of Eu^{3+} can also be determined based on the emission spectrum and lifetimes (τ) of the $^5D_0$ emitting level. Assuming that only nonradiative and radiative processes are essentially involved in the depopulation of the $^5D_0$ state, η can be expressed as:[25]

$$\eta = \frac{A_r}{A_r + A_{nr}} \quad (6)$$

Here, A_r and A_{nr} are radiative and nonradiative transition rates, respectively. A_r can be determined by the relative intensity of the $^5D_0 \rightarrow {}^7F_J$ (J = 0-4) transitions because of that $^5D_0 \rightarrow {}^7F_1$ is independent of the chemical environments around Eu^{3+} (it belong to the isolated magnetic dipole transition) and can be considered as internal reference (*ca.* 50 s^{-1}) for the whole spectrum, as shown in following equations:

$$A_{0J} = A_{01} \times \frac{I_{0J}}{I_{01}} \times \frac{V_{01}}{V_{0J}} \quad (7)$$

$$A_r = \sum A_{0J} = A_{00} + A_{01} + A_{02} + A_{03} + A_{04} \quad (8)$$

$$A_r + A_{nr} = \frac{1}{\tau} \quad (8)$$

Based on the values τ and the calculated A_r, η of ZnO@Zn(pdc)-Eu at different excitation wavelength are determined and given in Table S3. Results show that variation of excitation wavelength has slightly influence on η of ZnO@Zn(pdc)-Eu.

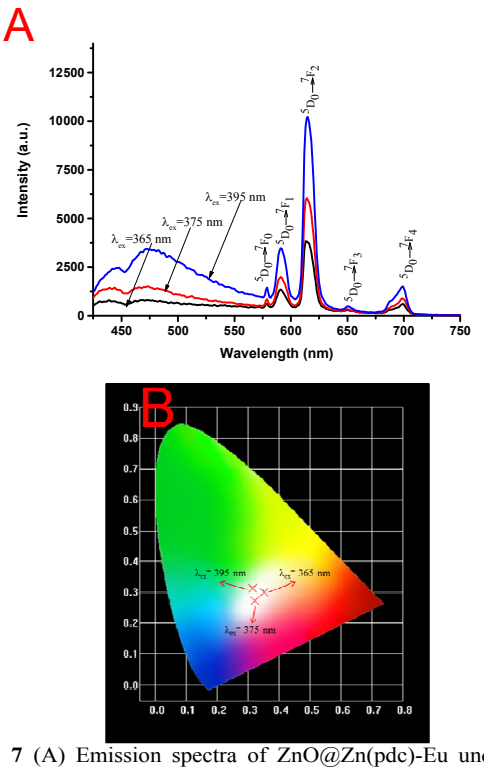

Figure 7 (A) Emission spectra of ZnO@Zn(pdc)-Eu under different excitation wavelength (365 nm, 375 nm, 395 nm); (B) CIE diagram of ZnO@Zn(pdc)-Eu under different excitation wavelength (365 nm, 375 nm, 395 nm).

In order to determine the stability of this white emission material, we adopt TG analysis (Figure S8), which confirms that ZnO@Zn(pdc)-Eu loses small molecule at two step with the weight loss of 12.42 % from 30 °C to 350 °C, indicating that the framework can be stable up to 350 °C. Also, a kind of simple white emission LED (WLED) assemblies using ZnO@Zn(pdc)-Eu were fabricated to verify the potential for emission device. The procedure employed a commercially available ultraviolet LED of 375 nm (Figure 8A) and an ZnO@Zn(pdc)-Eu sample as phosphor (Figure 8C). The resultant WLED shows bright warm white light at an applied voltage of 3.8V (Figure 8D). Under ambient condition, this fabricated WLED displays CIE, CCT values of (0.35, 0.41) and 5018 K, respectively. However, in the range of 300–500 K the luminescence intensity of the narrowband at 614 nm decreases with the increase of temperature (Figure S9), nearly cutting down a half every 50 K. Besides, ZnO@Zn(pdc)-Eu powder

has been manufactured on the LED emitting ultraviolet of 365 nm and 395 nm (Figure S10), showing strong cold white emission and weak warm white emission, respectively. On the basis of these results, it is clear that the ZnO@Zn(pdc)-Eu have potential for practical lighting applications under excitation of 375 nm.

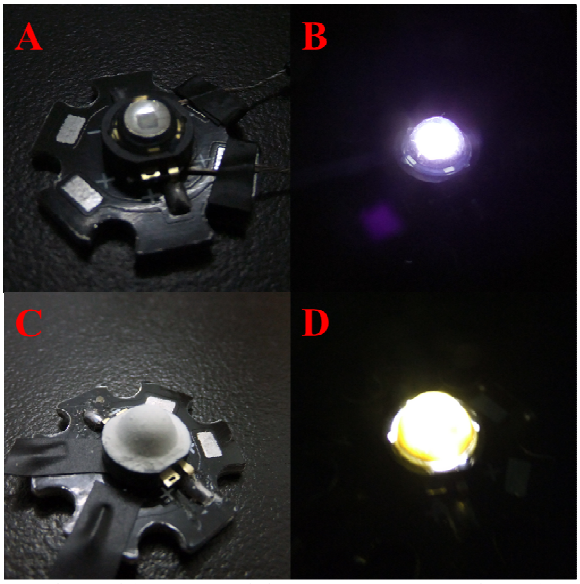

Figure 8 Photo of (A) LED emitting 375 nm (not turned on); (B) LED emitting 375 nm light (turned on); (C) LED coated with a thin layer of ZnO@Zn(pdc)-Eu (not turned on); (D) the coated LED turned on.

Conclusions

A series lanthanide ions (Eu^{3+}, Tb^{3+}, Sm^{3+}, Dy^{3+}) activated ZnO loaded zinc MOF is synthesized via solvothermal method. In addition, a hypothesis of ZnO forming mechanism is put forward, considering decomposition of zinc compounds caused by high-temperature as a main reason. Fluorescence spectra indicates that ZnO@Zn(pdc)-Ln (Ln = Eu, Tb, Sm, Dy) reveal characteristic emission under ultraviolet radiation, whose CIE coordinates fall in the region of reddish orange, yellowish green, orange, and yellow green, respectively. Beyond that, ZnO@Zn(pdc)-Eu can be exploiting as a potential luminescence material owing to its dual-emitting pathway luminescent properties. Moreover, a simple dip coating method is used to verify the potential of ZnO@Zn(pdc)-Eu fabricated as WLED devices. ZnO@Zn(pdc)-Eu coated commercial 375 nm LED presents warm white light with CIE coordinates of (0.35, 0.41) and CCT value of 5018 K.

Acknowledgements

This work was supported by the National Natural Science Foundation of China (91122003), Developing Science Funds of Tongji University and Science & Technology Commission of Shanghai Municipality (14DZ2261100).

Notes

[a] Department of Chemistry, and Shanghai Key Lab of Chemical Assessment and Sustainability, Tongji University, Siping Road 1239, Shanghai 200092, China. E-mail: byan@tongji.edu.cn; Tel: +86-21-65984663.

† Footnotes should appear here. These might include comments relevant to but not central to the matter under discussion, limited experimental and spectral data, and crystallographic data.

Electronic Supplementary Information (ESI) available: [details of any supplementary information available should be included here]. See DOI: 10.1039/b000000x/

References

1. (*a*) H. X. Deng, S. Grunder, K. E. Cordova, C. Valente, H. Furukawa, M. Hmadeh, F. Gandara, A. C. Whalley, Z. Liu, S. Asahina, H. Kazumori, M. O'Keeffe, O. Terasaki, J. F. Stoddart and O. M. Yaghi, *Science*, 2012, **336**, 1018; (*b*) H. Furukawa, K. E. Cordova, M. O'Keeffe and O. M. Yaghi, *Science*, 2013, **341**, 974; (*c*) G. K. H. Shimizu, J. M. Taylor and S. Kim, *Science*, 2013, **341**, 354.
2. (*a*) M. Gallo and D. Glossman-Mitnik, *J. Phys. Chem. C*, 2009, **113**, 6634; (*b*) S. Q. Ma and H. C. Zhou, *Chem. Commun.*, 2010, **46**, 44; (*c*) J. A. Mason, M. Veenstra and J. R. Long, *Chem. Sci.*, 2014, **5**, 32.
3. (*a*) T. W. Duan and B. Yan, *J. Mater. Chem. C*, 2014, **2**, 5098; (*b*) J. Heine and K. Muller-Buschbaum, *Chem. Soc. Rev.*, 2013, **42**, 9232; (*c*) Y. Lu and B. Yan, *Chem. Commun.*, 2014, **50**, 15443.
4. (*a*) Y. Zhou, H. H. Chen and B. Yan, *J. Mater. Chem. A*, 2014, **2**, 13691; (*b*) Y. Lu and B. Yan, *Chem. Commun.*, 2014, **50**, 13323; (*c*) J. N. Hao and B. Yan, *J. Mater. Chem. A*, 2014, **2**, 18018; (*d*) J. N. Hao and B. Yan, *J. Mater. Chem. C*, 2014, **2**, 6758.
5. (*a*) Y. Lu, B. Yan and J. L. Liu, *Chem. Commun.*, 2014, **50**, 9969; (*b*) J. Della Rocca, D. M. Liu and W. B. Lin, *Acct. Chem. Res.*, 2011, **44**, 957; (*c*) S. Keskin and S. Kizilel, *Ind Eng Chem. Res.*, 2011, **50**, 1799; (*d*) P. Horcajada, R. Gref, T. Baati, P. K. Allan, G. Maurin, P. Couvreur, G. Ferey, R. E. Morris and C. Serre, *Chem. Rev.*, 2012, **112**, 1232.
6. (*a*) Y. Zhou and B. Yan, *Inorg. Chem.*, 2014, **53**, 3456; (*b*) Y. Lu and B. Yan, *J. Mater. Chem. C*, 2014, **2**, 5526; (*c*) Y. Lu and B. Yan, *J. Mater. Chem. C*, 2014, **2**, 7411.
7. (*a*) M. D. Allendorf, C. A. Bauer, R. K. Bhakta and R. J. T. Houk, *Chem. Soc. Rev.*, 2009, **38**, 1330; (*b*) J. Rocha, L. D. Carlos, F. A. A. Paz and D. Ananias, *Chem. Soc. Rev.*, 2011, **40**, 926.
8. (*a*) X. Ma, X. Li, Y. E. Cha and L. P. Jin, *Cryst. Growth. Des.*, 2012, **12**, 5227; (*b*) C. Y. Sun, X. L. Wang, X. Zhang, C. Qin, P. Li, Z. M. Su, D. X. Zhu, G. G. Shan, K. Z. Shao, H. Wu and J. Li, *Nat. Commun.*, 2013, **4**, 2717; (*c*) J. He, M. Zeller, A. D. Hunter and Z. T. Xu, *J. Am. Chem. Soc.*, 2012, **134**, 1553; (*d*) D. F. Sava, L. E. S. Rohwer, M. A. Rodriguez and T. M. Nenoff, *J. Am. Chem. Soc.*, 2012, **134**, 3983.
9. (*a*) Y. J. Cui, H. Xu, Y. F. Yue, Z. Y. Guo, J. C. Yu, Z. X. Chen, J. K. Gao, Y. Yang, G. D. Qian and B. L. Chen, *J. Am. Chem. Soc.*, 2012, **134**, 3979; (*b*) Y. Liu, M. Pan, Q. Y. Yang, L. Fu, K. Li, S. C. Wei and C. Y. Su, *Chem. Mater.*, 2012, **24**, 1954.
10. (*a*) L. Ma, Y. C. Qiu, G. Peng, J. B. Cai, H. Deng and M. Zeller, *CrystEngComm.*, 2011, **13**, 3852; (*b*) W. T. Chen, R. H. Hu, Y. F. Wang, X. Zhang and J. Liu, *J. Solid. State Chem.*, 2014, **213**, 218; (*c*) J. Ruiz, G. Lorusso, M. Evangelisti, E. K. Brechin, S. J. A. Pope and E. Colacio, *Inorg. Chem.*, 2014, **53**, 3586; (*d*) M. L. Ma, J. H. Qin, C. Ji, H. Xu, R. Wang, B. J. Li, S. Q. Zang, H. W. Hou and S. R. Batten,

J. Mater. Chem. C, 2014, **2**, 1085; (*e*) X. Y. Xu and B. Yan, *Dalton Trans.*, 2015, 44, 1178.

11. (*a*) C. Bouvy, E. Chelnokov, R. Zhao, W. Marine, R. Sporken and B. L. Su, *Nanotechnology*, 2008, **19**, 105710; (*b*) S. J. So, H. J. Kim, D. H. Cha and C. S. Han, *J. Nanosci. Nanotechno.*, 2011, **11**, 847; (*c*) T. W. Duan and B. Yan, *Crystengcomm.*, 2014, **16**, 3395; (*d*) E. Pellicer, E. Rossinyol, M. Rosado, M. Guerrero, R. Domingo-Roca, S. Surinach, O. Castell, M. D. Baro, M. Roldan and J. Sort, *J. Colloid. Interf. Sci.*, 2013, **407**, 47.
12. (*a*) S. Saha, G. Das, J. Thote and R. Banerjee, *J. Am. Chem. Soc.*, 2014, **136**, 14845; (*b*) M. Ji, X. Lan, Z. P. Han, C. Hao and J. S. Qiu, *Inorg. Chem.*, 2012, **51**, 12389; (*c*) T. Kundu, S. C. Sahoo and R. Banerjee, *Cryst. Growth. Des.*, 2012, **12**, 2572.
13. (*a*) D. Esken, H. Noei, Y. M. Wang, C. Wiktor, S. Turner, G. Van Tendeloo and R. A. Fischer, *J. Mater. Chem.*, 2011, **21**, 5907; (*b*) F. F. Gao, G. S. Zhu, X. T. Li, B. S. Li, O. Terasaki and S. L. Qiu, *J. Phys. Chem. B*, 2001, **105**, 12704; (*c*) J. L. He, Y. Ba, C. I. Ratcliffe, J. A. Ripmeester, D. D. Klug, J. S. Tse and K. F. Preston, *J. Am. Chem. Soc.*, 1998, **120**, 10697.
14. (*a*) N. Sathitsuksanoh, D. Wang, H. Yang, Y. Lu and M. Park, *Acta. Mater.*, 2010, **58**, 373; (*b*) F. Wang, H. W. Song, G. H. Pan, L. B. Fan, Q. L. Dai, B. A. Dong, H. H. Liu, J. H. Yu, X. Wang and L. Li, *Mater. Res. Bull.*, 2009, **44**, 600; (*c*) J. Chen, Z. C. Feng, P. L. Ying and C. Li, *J. Phys. Chem. B*, 2004, **108**, 12669.
15. M. S. El-Shall, V. Abdelsayed, A. E. R. S. Khder, H. M. A. Hassan, H. M. El-Kaderi and T. E. Reich, *J. Mater. Chem.*, 2009, **19**, 7625.
16. (*a*) A. B. Djurisic and Y. H. Leung, *Small*, 2006, **2**, 944; (*b*) X. S. Fang, Y. Bando, U. K. Gautam, T. Y. Zhai, H. B. Zeng, X. J. Xu, M. Y. Liao and D. Golberg, *Crit. Rev. Solid. State.*, 2009, **34**, 190; (*c*) M. Willander, M. Q. Israr, J. R. Sadaf and O. Nur, *Nanophotonics*, 2012, **1**, 99; (*d*) P. A. Rodnyi and I. V. Khodyuk, *Opt. Spectrosc.*, 2011, **111**, 776.
17. S. Bordiga, C. Lamberti, G. Ricchiardi, L. Regli, F. Bonino, A. Damin, K. P. Lillerud, M. Bjorgen and A. Zecchina, *Chem. Commun.*, 2004, 2300.
18. P. L. Feng, J. J. Perry, S. Nikodemski, B. W. Jacobs, S. T. Meek and M. D. Allendorf, *J. Am. Chem. Soc.*, 2010, **132**, 15487.
19. W. W. Zhan, Q. Kuang, J. Z. Zhou, X. J. Kong, Z. X. Xie and L. S. Zheng, *J. Am. Chem. Soc.*, 2013, **135**, 1926.
20. D. K. Lee, J. H. Park, J. Il Choi, Y. Lee, S. J. Kim, G. H. Lee, Y. H. Kim and J. K. Kang, *Nanoscale*, 2014, **6**, 10995.
21. V. I. Isaeva, E. V. Belyaeva, A. N. Fitch, V. V. Chernyshev, S. N. Klyamkin and L. M. Kustov, *Cryst. Growth. Des.*, 2013, **13**, 5305.
22. T. P. Petersen, A. F. Larsen, A. Ritzen and T. Ulven, *J. Org. Chem.*, 2013, **78**, 4190.
23. M. E. Fragala, Y. Aleeva and G. Malandrino, *Superlattice. Microst.*, 2010, **48**, 408.
24. (*a*) K. H. Kwon, W. Bin Im, H. S. Jang, H. S. Yoo and D. Y. Jeon, *Inorg. Chem.*, 2009, **48**, 11525; (*b*) J. Y. Han, W. B. Im, G. Y. Lee and D. Y. Jeon, *J. Mater. Chem.*, 2012, **22**, 8793.
25. (*a*) Y. J. Li and B. Yan, *Inorg. Chem.*, 2009, **48**, 8276; (*b*) B. Yan and Y. J. Li, *J. Mater. Chem.*, 2011, **21**, 18454.

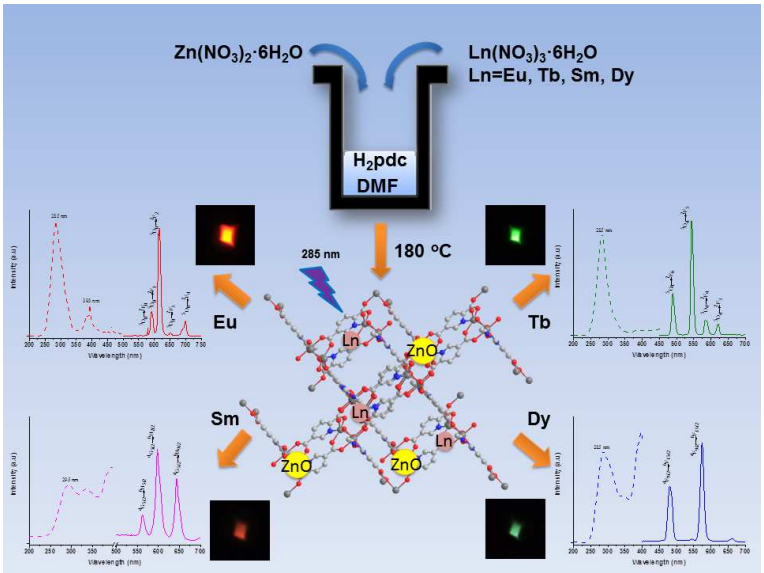

A series of hybrids based on lanthanide ions activated zinc metallic organic framework of 2,5-pyridinedicarboxylate (ZnO@Zn(pdc)-Ln, Ln = Eu, Tb, Sm, Dy) have been synthesized by coordination reaction under solvothermal conditions. Zinc oxide is formed in the framework of lanthanide doped zinc centered MOFs due to decomposition of zinc compounds caused by alkaline environment and high-temperature. Photophysical properties of these hybrid materials are investigated in details and reveal that characteristic emission line of corresponding Ln^{3+} ion is appeared under ultraviolet radiation .